

A three-dimensional lattice gas model for amphiphilic fluid dynamics

Bruce M. Boghosian,

Center for Computational Science, Boston University,

3 Cummington Street, Boston, Massachusetts 02215, U.S.A.

`bruceb@bu.edu`

Peter V. Coveney,

Centre for Computational Science, Queen Mary and Westfield College,

University of London, Mile End Road,

London E1 4NS, U.K.

`p.v.coveney@qmw.ac.uk`

and

Peter J. Love

Theoretical Physics, Department of Physics, University of Oxford,

1 Keble Road, Oxford, OX1 3NP, UK

`p.love1@physics.oxford.ac.uk`

January 14, 2014

Abstract

We describe a three-dimensional hydrodynamic lattice-gas model of amphiphilic fluids. This model of the non-equilibrium properties of oil-water-surfactant systems, which is a non-trivial extension of an earlier two-dimensional realisation due to Boghosian, Coveney and Emerton [2], can be studied effectively only when it is implemented using high-performance computing and visualisation techniques. We describe essential aspects of the model's theoretical basis and computer implementation, and report on the phenomenological properties of the model which confirm that it correctly captures binary oil-water and surfactant-water behaviour, as well as the complex phase behaviour of ternary amphiphilic fluids.

1 Introduction

Oil and water are immiscible fluids under normal conditions of temperature and pressure. Their phase separation behaviour in binary mixtures has been extensively studied both experimentally and theoretically, and has become a testbed for many fluid simulation methods [3,15]. However, the addition of amphiphile (or surfactant) to these systems produces much more complex behaviour. A general review of the equilibrium phase behaviour of these fluids and theoretical methods for studying them was provided by Gompper and Schick [14]. The complex phase behaviour of binary and ternary amphiphilic fluids arises as a result of the physical and chemical properties of amphiphilic molecules. Amphiphile molecules possess a hydrophilic head and a hydrophobic tail. As a result it is usually energetically favourable for the amphiphile molecules to be adsorbed at oil-water interfaces, effectively reducing the interfacial tension. Complex morphologies, termed mesophases, occur in both binary (surfactant and water or oil) and ternary amphiphilic systems. In general these structures depend on the concentration and chemical nature of the surfactant molecules (length of hydrocarbon tail, size of head group, and so on) as well as on the temperature. The equilibrium phase diagrams for these systems have been obtained from experimental investigation [16]. Of considerable interest are the *microemulsion* phases; an example is the very low surface tension which exist between the “middle” microemulsion phase and the bulk oil and water phases [14], but there are many other fascinating phenomena including the viscoelastic properties of wormlike micelles and the formation of vesicles [8,14]. Their intrinsic complexity and wide application make these systems appropriate for detailed scientific inquiry. Although the equilibrium phase behaviour of these systems is well understood, relatively little work has been done on their non-equilibrium properties. Much of the work which has addressed these dynamic properties has been based on molecular dynamics methods [18,19,22]. However, such atomistic approaches are too computationally demanding to allow investigation of the important large-time dynamics and extended spatial structures of these systems. Indeed, a large part of the fascination of amphiphilic fluids is related to the dependence of their macroscopic properties on the underlying molecular and mesoscopic dynamics, which calls for the development of techniques which can efficiently bridge the length and time scale gaps from micro to macro.

In the present paper we report on the formulation and implementation of a three-dimensional hydrody-

dynamic lattice gas model, which has been extensively studied in two dimensions [2, 9–12]. Compared with molecular dynamics the computational simplicity of lattice gases makes them an ideal method for modelling complex fluid behaviour from the mesoscale upwards. They have been used extensively for modelling hydrodynamics since Frisch, Hasslacher, and Pomeau [13], and Wolfram [21] showed that it is possible to simulate the incompressible Navier-Stokes equations using discrete boolean elements on a lattice. Rothman and Keller subsequently generalised the basic lattice gas method to allow simulation of immiscible fluids [20], and we have used their model as the starting point for our own work.

Notwithstanding the simplifications engendered by invoking the lattice-gas paradigm, the simulation of the non-equilibrium behavior of ternary amphiphilic fluids in three dimensions is a highly demanding area of computational science; indeed, the results presented in this paper have been made possible only by the recent availability of sufficiently powerful parallel computing architectures, as well as sophisticated visualisation methods.

The purpose of the present paper is to describe the implementation of our three-dimensional model, and to establish its validity. In particular, we show that our model can reproduce the well known features of amphiphilic fluid phenomenology. In Sections 2 and 3 we describe our model, emphasising in particular the differences between the 2D and 3D lattice-gas realisations, and briefly describe the computational requirements of the work. Section 4 outlines the basic structure of the algorithm, while Section 5 specifies the coupling constants which are used in our simulations. The results of the simulations are presented in Section 6. These simulations demonstrate the ability of our model to represent binary immiscible behaviour, binary water-surfactant self-assembly and ternary amphiphilic behaviour. Finally we close the paper with some conclusions in Section 7.

2 Amphiphilic Lattice-Gas Dynamics

Our lattice-gas model of amphiphilic fluids consists of three different species of particles moving about on a D -dimensional lattice \mathcal{L} in discrete time steps. The three species are the two immiscible fluids (oil and water) denoted by red (R) and blue (B) colours, respectively, and the amphiphile A . Lattice-gas particles

can have velocities \mathbf{c}_i , where $1 \leq i \leq b$, and b is the number of velocities per site. We shall measure discrete time in units of one lattice update, so that a particle emerging from a collision at site \mathbf{x} and time t with velocity \mathbf{c}_i will stream to site $\mathbf{x} + \mathbf{c}_i$ where it may undergo the next collision. The \mathbf{c}_i must thus be integer multiples of the lattice vectors; it is also possible to have $\mathbf{c}_i = \mathbf{0}$ for some i to allow for “rest particles” with zero speed.

We let $n_i^\alpha(\mathbf{x}, t) \in \{0, 1\}$ denote the presence (1) or absence (0) of a particle of species $\alpha \in \{R, B, A\}$ with velocity \mathbf{c}_i , at lattice site $\mathbf{x} \in \mathcal{L}$ and time step t . The $n_i^\alpha(\mathbf{x}, t)$ are not all independent since an “exclusion rule” is enforced whereby there can be no more than one particle of a given velocity at a given lattice site at a given time. The collection of all $n_i^\alpha(\mathbf{x}, t)$ for $1 \leq i \leq b$ shall be denoted by $\mathbf{n}^\alpha(\mathbf{x}, t)$. This is not to be confused with the total number of particles of a given colour,

$$n^\alpha(\mathbf{x}, t) \equiv \sum_{i=1}^b n_i^\alpha(\mathbf{x}, t). \quad (1)$$

Likewise, we shall sometimes need the *colour charge* associated with a given site,

$$q_i(\mathbf{x}, t) \equiv n_i^R(\mathbf{x}, t) - n_i^B(\mathbf{x}, t), \quad (2)$$

as well as the total colour charge at a site,

$$q(\mathbf{x}, t) \equiv \sum_{i=1}^b q_i(\mathbf{x}, t). \quad (3)$$

Finally, the collection of all $\mathbf{n}^\alpha(\mathbf{x}, t)$ for $\alpha \in \{R, B, A\}$ will be called the *population state* of the site; it is denoted by

$$\mathbf{n}(\mathbf{x}, t) \in \mathcal{N} \quad (4)$$

where we have introduced the notation \mathcal{N} for the (finite) set of all distinct population states.

In addition to the specification of the particle populations at a site, the amphiphile particles have an orientation, denoted by $\boldsymbol{\sigma}_i(\mathbf{x}, t)$. This orientation vector, which has fixed magnitude σ , specifies the orientation of the director of the amphiphile particle at site \mathbf{x} and time step t with velocity \mathbf{c}_i . (Of course, if there is no amphiphile particle with that site, time step and velocity, then the value of $\boldsymbol{\sigma}_i(\mathbf{x}, t)$ there is not defined.) In our work, the values of the $\boldsymbol{\sigma}_i(\mathbf{x}, t)$ vectors may vary continuously¹ on a $(D-1)$ -sphere, denoted by S^{D-1} ;

¹It is also possible to construct models with discrete set of values for the $\boldsymbol{\sigma}_i$, but we do not consider that possibility in this paper.

thus, they take their values on a circle for $D = 2$ and a sphere for $D = 3$. The collection of the b vectors $\boldsymbol{\sigma}_i(\mathbf{x}, t)$ at a given site \mathbf{x} and time step t is called the *orientation state*,

$$\boldsymbol{\Sigma}(\mathbf{x}, t) \equiv (\boldsymbol{\sigma}_1(\mathbf{x}, t), \boldsymbol{\sigma}_2(\mathbf{x}, t), \dots, \boldsymbol{\sigma}_b(\mathbf{x}, t)) \in \bigotimes^b S^{D-1}, \quad (5)$$

where \bigotimes^b denotes the b -fold Cartesian product. This is not to be confused with the *total director* of a site

$$\boldsymbol{\sigma}(\mathbf{x}, t) \equiv \sum_{i=1}^b \boldsymbol{\sigma}_i(\mathbf{x}, t). \quad (6)$$

We shall also find it useful to define the following scalar director field

$$S(\mathbf{x}, t) \equiv \sum_{i=1}^b \mathbf{c}_i \cdot \boldsymbol{\sigma}_i(\mathbf{x}, t). \quad (7)$$

Together, the population state and the orientation state completely specify (in fact, as noted above, they overspecify) the *total state* of the site,

$$s \equiv (\mathbf{n}, \boldsymbol{\Sigma}), \quad (8)$$

where we have omitted the site and time-step specification for brevity.

The time evolution of the system is an alternation between a streaming or *propagation* step and a *collision* step. In the first of these, the particles move in the direction of their velocity vectors to new lattice sites. This is described mathematically by the replacements

$$n_i^\alpha(\mathbf{x} + \mathbf{c}_i, t + 1) \leftarrow n_i^\alpha(\mathbf{x}, t) \quad (9)$$

$$\boldsymbol{\sigma}_i(\mathbf{x} + \mathbf{c}_i, t + 1) \leftarrow \boldsymbol{\sigma}_i(\mathbf{x}, t), \quad (10)$$

for all $\mathbf{x} \in \mathcal{L}$, $1 \leq i \leq b$ and $\alpha \in \{R, B, A\}$. That is, particles with velocity \mathbf{c}_i simply move from point \mathbf{x} to point $\mathbf{x} + \mathbf{c}_i$ in one time step.

In the collision step, the newly arrived particles interact, resulting in new momenta and directors. The collisional change in the state of a lattice site \mathbf{x} is required to conserve the mass of each species present

$$\rho^\alpha(\mathbf{x}, t) \equiv \sum_i^b n_i^\alpha(\mathbf{x}, t), \quad (11)$$

as well as the D -dimensional momentum vector

$$\mathbf{p}(\mathbf{x}, t) \equiv \sum_\alpha \sum_i^b \mathbf{c}_i n_i^\alpha(\mathbf{x}, t) \quad (12)$$

(where we have assumed for simplicity that the particles all carry unit mass). Thus, the set \mathcal{N} of population states at each site is partitioned into *equivalence classes* of population states having the same values of these conserved quantities. For a site with given masses $\boldsymbol{\rho} \equiv (\rho^R, \rho^B, \rho^A)$ and momentum \mathbf{p} , we denote the set of allowed population states by $E(\boldsymbol{\rho}, \mathbf{p}) \subset \mathcal{N}$. Since the conservation laws do not restrict the orientations of the directors, the set of allowed total states is then

$$\mathcal{E}(\boldsymbol{\rho}, \mathbf{p}) = E(\boldsymbol{\rho}, \mathbf{p}) \bigotimes_{i=1}^b S^{D-1}. \quad (13)$$

Given a precollision total state $s \in E(\boldsymbol{\rho}, \mathbf{p})$ with masses $\boldsymbol{\rho}$ and momentum \mathbf{p} , the postcollision total state s' must belong to the set

$$s' = (\mathbf{n}', \boldsymbol{\Sigma}') \in \mathcal{E}(\boldsymbol{\rho}(s), \mathbf{p}(s)). \quad (14)$$

Henceforth, primed quantities are understood always to refer to the postcollision state. In our model, s' is sampled from a probability density $\mathcal{P}(s')$, sometimes equivalently denoted $\mathcal{P}(\mathbf{n}', \boldsymbol{\Sigma}')$, imposed upon this set. We assume that the characteristic time for collisional and orientational relaxation is sufficiently fast in comparison to that of the propagation that we can model this probability density as the Gibbsian equilibrium corresponding to a Hamiltonian function; that is

$$\mathcal{P}(s') = \frac{1}{\mathcal{Z}} \exp[-\beta H(s')], \quad (15)$$

where β is an inverse temperature, $H(s')$ is the energy associated with collision outcome s' , and \mathcal{Z} is the equivalence-class partition function,

$$\mathcal{Z}(\boldsymbol{\rho}, \mathbf{p}, \beta) \equiv \sum_{\mathbf{n}' \in E(\boldsymbol{\rho}, \mathbf{p})} \int d\boldsymbol{\Sigma}' \exp[-\beta H(s')], \quad (16)$$

and we have defined the measure on the set of orientational states

$$\int d\boldsymbol{\Sigma} \equiv \bigotimes_{i=1}^b \int d\boldsymbol{\sigma}_i. \quad (17)$$

In practice, we sample $s' = (\mathbf{n}', \boldsymbol{\Sigma}')$ by first sampling the postcollision population state \mathbf{n}' from the reduced probability density

$$P(\mathbf{n}') = \int d\boldsymbol{\Sigma}' \mathcal{P}(s'). \quad (18)$$

We then sample the postcollision orientation state by sampling the b orientations $\boldsymbol{\sigma}'_i$ from each of

$$\pi_i(\boldsymbol{\sigma}'_i) = \prod_{j \neq i}^b \int d\boldsymbol{\sigma}'_j \mathcal{P}(\mathbf{n}', \boldsymbol{\Sigma}') . \quad (19)$$

for $1 \leq i \leq b$; these are, as we shall see, independent distributions, so the b samples may each be taken without regard for the other outcomes. This completes the collision process.

3 Local Amphiphilic Lattice-Gas Hamiltonian

It remains to specify the local Hamiltonian used in the collision outcome selection process. Such a Hamiltonian has been derived and described in detail for the two-dimensional version of the model [2], and we use the same one here ². It is

$$H(s') = \mathbf{J} \cdot (\alpha \mathbf{E} + \mu \mathbf{P}) + \boldsymbol{\sigma}' \cdot (\epsilon \mathbf{E} + \zeta \mathbf{P}) + \mathcal{J} : (\epsilon \mathcal{E} + \zeta \mathcal{P}) + \frac{\delta}{2} \mathbf{v}(\mathbf{x}, t)^2, \quad (20)$$

where we have introduced the *colour flux* vector of an outgoing state

$$\mathbf{J}(\mathbf{x}, t) \equiv \sum_{i=1}^b \mathbf{c}_i q'_i(\mathbf{x}, t), \quad (21)$$

the *dipolar flux* tensor of an outgoing state

$$\mathcal{J}(\mathbf{x}, t) \equiv \sum_{i=1}^b \mathbf{c}_i \boldsymbol{\sigma}'_i(\mathbf{x}, t), \quad (22)$$

the *colour field* vector

$$\mathbf{E}(\mathbf{x}, t) \equiv \sum_{i=1}^b \mathbf{c}_i q(\mathbf{x} + \mathbf{c}_i, t), \quad (23)$$

the *dipolar field* vector

$$\mathbf{P}(\mathbf{x}, t) \equiv - \sum_{i=1}^b \mathbf{c}_i S(\mathbf{x} + \mathbf{c}_i, t), \quad (24)$$

the *colour field gradient* tensor

$$\mathcal{E}(\mathbf{x}, t) \equiv \sum_{i=1}^b \mathbf{c}_i \mathbf{E}(\mathbf{x} + \mathbf{c}_i, t), \quad (25)$$

²Actually, the forms given for the various fields in reference [2] are somewhat more general than those given here. In this presentation we restrict ourselves to nearest neighbour interactions for simplicity.

the *dipolar field gradient* tensor ³

$$\mathcal{P}(\mathbf{x}, t) \equiv - \sum_{i=1}^b \mathbf{c}_i \mathbf{c}_i S(\mathbf{x} + \mathbf{c}_i, t), \quad (26)$$

and the kinetic energy of the particles at a site.

$$\frac{\delta}{2} |\mathbf{v}(\mathbf{x}, t)|^2, \quad (27)$$

where \mathbf{v} is the average velocity of all particles at a site, the mass of the particles is taken as unity, and α , μ , ϵ , ζ and δ are coupling constants.

We note that the change in kinetic energy was not included by Rothman and Keller in their immiscible lattice gas model. We include it here for completeness, and set $\delta = 1.0$; although it will not affect the equilibrium properties of the model, it may impact the non-equilibrium properties. It should be further noted that the inverse temperature-like parameter β is not related in the conventional way to the kinetic energy. For a discussion of the introduction of this parameter into lattice gases to reproduce critical behaviour we refer the reader to the original work by Chan and Liang [5].

Eqs. (20 - 26) were derived by assuming that there is an interaction potential between colour charges, and that the directors are like “colour dipoles” in this context [2]. The terms containing α models the interaction of colour charges with surrounding colour charges as in the original Rothman-Keller model [20]; those containing μ model the interaction of colour charges with surrounding colour dipoles; those containing ϵ model the interaction of colour dipoles with surrounding colour charges (alignment of surfactant molecules across oil-water interfaces); those containing ζ model the interaction of colour dipoles with surrounding colour dipoles (interfacial bending energy or “stiffness”).

Note that the field quantities depend only on the precollision state, whereas the flux quantities depend on the postcollision state. Thus, the fields may be computed once at every site, just after the propagation step. The fluxes, on the other hand, must be computed for each possible outgoing state. It follows that the Hamiltonian may be written in the form

$$H(s') = H_0(\mathbf{n}') + \sum_{i=1}^b n_i^{A'} \mathbf{A}_i \cdot \boldsymbol{\sigma}'_i, \quad (28)$$

³Note that this definition differs from that used in the reference [2]. The two definitions can be reconciled by a redefinition of the coupling constants.

where we have defined

$$H_0(\mathbf{n}') \equiv \mathbf{J} \cdot (\alpha \mathbf{E} + \mu \mathbf{P}) \quad (29)$$

and

$$\mathbf{A}_i \equiv \sigma [\epsilon \mathbf{E} + \zeta \mathbf{P} + (\epsilon \mathcal{E} + \zeta \mathcal{P}) \cdot \mathbf{c}_i]. \quad (30)$$

The reduced probability density for \mathbf{n}' is then

$$P(\mathbf{n}') = \int d\Sigma' \mathcal{P}(s') = \frac{\exp[-\beta H_0(\mathbf{n}')] }{\mathcal{Z}} \prod_{i=1}^b \int d\sigma'_i \exp(-\beta n_i^{A'} \mathbf{A}_i \cdot \boldsymbol{\sigma}_i), \quad (31)$$

and this demands evaluation of integrals of the form

$$\int d\boldsymbol{\sigma} \exp(-n\beta \mathbf{A} \cdot \boldsymbol{\sigma}). \quad (32)$$

In two dimensions ($D = 2$), we can adopt a polar coordinate θ , chosen so that $\theta = 0$ is the direction of \mathbf{A} , so that this integral becomes

$$\int_0^{2\pi} d\theta \exp(-n\beta\sigma|\mathbf{A}|\cos\theta) = 2\pi I_0(n\beta\sigma|\mathbf{A}|), \quad (33)$$

where I_0 is the modified Bessel function of the first kind [2]. So, from from Eq. (18), we get the reduced probability density

$$P(\mathbf{n}') = \frac{(2\pi)^b \exp[-\beta H_0(\mathbf{n}')] }{\mathcal{Z}} \prod_{i=1}^b I_0(n_i^{A'} \beta\sigma|\mathbf{A}_i|) \quad (34)$$

which must be evaluated numerically for every possible outgoing state.

In three dimensions ($D = 3$), we adopt spherical coordinates with polar axis in the direction of \mathbf{A} , so that the integral over the orientational degrees of freedom is of the form

$$\int_0^{2\pi} d\phi \int_0^\pi d\theta \sin\theta \exp(-n\beta\sigma|\mathbf{A}|\cos\theta) = 4\pi \begin{cases} 1 & \text{if } n = 0 \\ \frac{\sinh(\beta\sigma|\mathbf{A}|)}{\beta\sigma|\mathbf{A}|} & \text{if } n = 1, \end{cases} \quad (35)$$

where θ is the colatitude and ϕ is the azimuthal angle. The reduced probability density of Eq. (18) is then

$$P(\mathbf{n}') = \frac{(4\pi)^b \exp[-\beta H_0(\mathbf{n}')] }{\mathcal{Z}} \prod_{i=1}^b \left\{ 1 + n_i^{A'} \left[\frac{\sinh(\beta\sigma|\mathbf{A}_i|)}{\beta\sigma|\mathbf{A}_i|} - 1 \right] \right\}. \quad (36)$$

Once the reduced probability is sampled from $P(\mathbf{n}')$, we turn our attention to the determination of the new orientation state. For $D = 2$, the reduced probability density for the angle θ'_i is given by

$$\pi_i(\theta'_i) = \frac{\exp(-\beta\sigma|\mathbf{A}_i|\cos\theta'_i)}{2\pi I_0(\beta\sigma|\mathbf{A}_i|)}. \quad (37)$$

For $D = 3$, the probability density for the colatitude θ'_i and azimuthal angle ϕ'_i is then

$$\pi_i(\theta'_i, \phi'_i) = \frac{\exp(-\beta\sigma |\mathbf{A}_i| \cos \theta'_i) \sin \theta'_i}{4\pi \left[\frac{\sinh(\beta\sigma |\mathbf{A}_i|)}{\beta\sigma |\mathbf{A}_i|} \right]}. \quad (38)$$

4 Algorithmic Considerations

A computer implementation of our hydrodynamic lattice-gas model requires a choice of data representation for the population state \mathbf{n} and the orientation state Σ . We consider these in turn. As noted above, the variables $n_i^\alpha(\mathbf{x}, t)$ are not all independent because of the “exclusion rule” that only one particle of any type may have a given velocity i at a given site \mathbf{x} and time step t . Thus, it is inefficient to store these variables directly. Rather, we note that for a given i , \mathbf{x} and t there are precisely four possibilities: there can be a particle of type R , type B , type A , or nothing at all. These four possibilities can be encoded in two bits of information as follows:

High Bit	Low Bit	Description
0	0	Nothing
0	1	R particle
1	0	B particle
1	1	A particle

Thus, the population state of a given site can be represented by $2b$ bits of information. For $D = 2$, our current implementation uses a triangular lattice (coordination number 6) and one rest particle, so $b = 7$ and 14 bits are needed to store the population state [2]. For $D = 3$, our current implementation uses a projected face-centered hypercubic (PFCHC) lattice (coordination number 24) and two rest particles, so $b = 26$ and 52 bits are needed to store the population state [1, 13]. The PFCHC lattice will be described in some detail later in this section. For now we note that in either case, the population state easily fits in a single integer variable; more precisely, for $D = 2$ it fits in a “short” integer of 16 bits, and for $D = 3$ it fits in a “double-precision” integer of 64 bits.

The orientation state requires much more storage because we have chosen to allow the orientation angles to be continuous⁴. For $D = 2$ we must store the b polar angles θ_i , each as an IEEE-format, single precision, floating-point variable of 32 bits. For $D = 3$ we must likewise store the two spherical angles for each velocity for a total of $2b$ floating-point variables. While it is true that these angular variables are not defined unless the corresponding $n_i^{A'} = 1$, our current implementation provides for storage for all angles at all sites and velocities, because the computational price of dynamically allocating and deallocating variables was not thought to be worth the savings in storage; for very low surfactant concentrations, this assumption may be invalid, and so the existing code might be improved.

In a language that allows for user-defined types, such as Fortran 90, C++ or Java, it is useful to create a type for the total state of a site that includes both the population and orientation information. Given this data representation, the implementation of the propagation step is fairly obvious. The substitutions of Eqs. (9) and (10) are made throughout the lattice. In Fortran 90, the CSHIFT intrinsic accomplishes periodic shifts on arrays, and it is natural to use this to construct a subroutine that accepts an array of type 'total state' and performs the propagation procedure on this array as a side effect. The above-described representation for the population state is somewhat inconvenient in this regard, as the bit pairs corresponding to a particular velocity must be extracted from the integer variable before it is shifted in that direction. When the propagation step is completed, the new fields S , \mathbf{E} , \mathbf{P} , \mathcal{E} and \mathcal{P} are computed at each site using Eqs. (7) and (23) - (26).

Next, the possible outcomes for the population state are enumerated using a lookup-table procedure. A list of all possible outgoing states that has been sorted according to equivalence class $E(\boldsymbol{\rho}, \mathbf{p})$ is precomputed and stored. This list is of length $2^{14} = 16384$ for the $D = 2$ case. A full list for the 52-bit population state representation in $D = 3$ would have length 2^{52} and this is obviously much too large to store on any existing or contemplated computer; a method of shortening this list will be described below. For now, assume that such a list could be stored, and that two other lists of the same size could be maintained that accept the current population state \mathbf{n} as a key, and return a pointer to the initial position and the number of elements of the

⁴As noted in an earlier footnote, this choice is not thought to be essential, and it is possible that much storage space may be saved by requiring the orientation angles to be discrete.

equivalence class $E(\boldsymbol{\rho}, \mathbf{p})$ in the table of sorted states. This makes it possible to enumerate the postcollision states \mathbf{n}' that respect the required conservation laws. Note that the length of this list may vary from site to site.

Next, each site loops over its set $E(\boldsymbol{\rho}, \mathbf{p})$ of allowed postcollision states and computes the outgoing colour flux vector \mathbf{J} and the b auxiliary vectors \mathbf{A}_i for each one of them, using Eqs. (21) and (30) respectively. These are then used to compute the reduced probability density $P(\mathbf{n}')$, given by Eq. (34) for $D = 2$, or Eq. (36) for $D = 3$. Given these probabilities, a final population state \mathbf{n}' is sampled.

Once \mathbf{n}' is known, the \mathbf{A}_i are recalculated for that final state, and the final orientation angles are sampled from Eq. (37) for $D = 2$, or Eq. (38) for $D = 3$. In the latter case, we note that $\pi_i(\theta'_i, \phi'_i)$ is independent of ϕ'_i so this may simply be sampled uniformly in $(0, 2\pi)$. The colatitude θ'_i is then found by equating its cumulative distribution function to a random number r uniformly distributed between 0 and 1, and solving for θ'_i . The result is

$$\theta'_i = \arccos \left\{ \frac{-1}{\beta\sigma|\mathbf{A}_i|} \ln \left[r e^{+\beta\sigma|\mathbf{A}_i|} + (1-r) e^{-\beta\sigma|\mathbf{A}_i|} \right] \right\}. \quad (39)$$

For $D = 2$, the sampling procedure is not so simple, because of the integral leading to the modified Bessel function. In this case we proceed numerically; for small values of the parameter $\beta\sigma|\mathbf{A}_i|$, we approximate the distribution by a Gaussian centered at its maximum, and for small values of $\beta\sigma|\mathbf{A}_i|$ we employ rejection sampling [2].

It remains to describe the PFCHC lattice and our method for making the size of the lookup table more manageable. The face-centered hypercubic (FCHC) lattice is a regular, self-dual lattice in four dimensions with coordination number 24. It can be described as all integer-valued tetrads (i, j, k, l) such that $i + j + k + l$ is even. The motivation for using this lattice is that it is known to yield isotropic Navier-Stokes behaviour for a single-phase fluid [13].

The lattice vectors are then the 24 neighbours of the site $(0, 0, 0, 0)$, and these can be partitioned into a subset of eight lattice vectors called Group 1, namely $(\pm 1, 0, 0, \pm 1)$ and $(0, \pm 1, \pm 1, 0)$, a subset of eight lattice vectors called Group 2, namely $(0, \pm 1, 0, \pm 1)$ and $(\pm 1, 0, \pm 1, 0)$, and a subset of eight lattice vectors called Group 3, namely $(0, 0, \pm 1, \pm 1)$ and $(\pm 1, \pm 1, 0, 0)$. The virtue of this partition is that the sixteen lattice

vectors of any two groups lie on the corners of a regular four-dimensional hypercube, and the eight lattice vectors of the remaining group point to the face centers of that hypercube [1].

The projection of the FCHC lattice to the three-dimensional PFCHC lattice can be accomplished by simply ignoring the fourth coordinate of the 24 vectors described above. The partition into three groups of eight vectors is still useful to maintain, as we shall see. One feature of this projection is that distinct vectors of the FCHC lattice can project to the same vector on the PFCHC lattice; for example, $(1, 0, 0, 1)$ and $(1, 0, 0, -1)$ both project to $(1, 0, 0)$. We take these 24 three-vectors as the particle velocities in our $D = 3$ model, and add two rest particles to them for a total of 26 particle velocities ($b = 26$). In our computer implementation, we append the (same) two rest particles to each of our three groups of eight lattice vectors, to obtain three groups of ten velocities ($b = 10$) each. The idea is then to allow collisions within each group of ten velocities separately, updating the state of the rest particles in all three groups whenever they change, thereby letting the rest particles provide mass and momentum transfer between the three groups. The three sets of velocities are summarized in the following table:

Group	Lattice Vector	Components x, y, z	Group	Lattice Vector	Components x, y, z	Group	Lattice Vector	Components x, y, z
1	\mathbf{c}_1	1, 0, 0	2	\mathbf{c}_1	0, 1, 0	3	\mathbf{c}_1	0, 0, 1
	\mathbf{c}_2	1, 0, 0		\mathbf{c}_2	0, 1, 0		\mathbf{c}_2	0, 0, 1
	\mathbf{c}_3	-1, 0, 0		\mathbf{c}_3	0, -1, 0		\mathbf{c}_3	0, 0, -1
	\mathbf{c}_4	-1, 0, 0		\mathbf{c}_4	0, -1, 0		\mathbf{c}_4	0, 0, -1
	\mathbf{c}_5	0, 1, 1		\mathbf{c}_5	1, 0, 1		\mathbf{c}_5	1, 1, 0
	\mathbf{c}_6	0, 1, -1		\mathbf{c}_6	-1, 0, 1		\mathbf{c}_6	1, -1, 0
	\mathbf{c}_7	0, -1, 1		\mathbf{c}_7	1, 0, -1		\mathbf{c}_7	-1, 1, 0
	\mathbf{c}_8	0, -1, -1		\mathbf{c}_8	-1, 0, -1		\mathbf{c}_8	-1, -1, 0
	\mathbf{c}_9	0, 0, 0		\mathbf{c}_9	0, 0, 0		\mathbf{c}_9	0, 0, 0
	\mathbf{c}_{10}	0, 0, 0		\mathbf{c}_{10}	0, 0, 0		\mathbf{c}_{10}	0, 0, 0

Since two bits of information are required to represent the population state for each velocity, a total of 20 bits will specify the state within each group. This results in tables of length $2^{20} = 1048576$. Since the results can be stored as single-precision (32-bit, or four-byte) integers, the tables each require a total of 4 Mbytes of storage. Since there are three tables, as described above, a grand total of 12 Mbytes are devoted to table storage. This amount of storage is not a significant problem on modern multiprocessor supercomputers.

Once again, the use of user-defined types can simplify the implementation of the above decomposition. The population state can be made a user-defined type, constructed from three integer variables. Subroutines for propagation, table lookup, and other collision-related operations can then be overloaded to accommodate the new type.

Despite the advantage gained by using the hydrodynamic lattice gas method described above, the simulation of large three dimensional amphiphilic systems remains extremely computationally demanding. The algorithm described above has been implemented in Fortran90, and parallelised using the MPI (Message Passing Interface) library. Simulations for the parameter search described in Section 5 were performed on a 512 processor Cray T3D at the Edinburgh Parallel Computing Centre (EPCC). The code was then ported to SGI Origin 2000 machines at Schlumberger Cambridge Research, the National Computational Science Alliance (NCSA) in Illinois, and at the Oxford Supercomputing Centre. The Cray T3D and T3E systems are Massively Parallel Processor (MPP) machines, whereas the SGI O2000 machines have cache-coherent Non-Uniform Memory Architecture (ccNUMA). These two parallel architectures are very different, and the ease of moving from one to the other illustrates the portability of modern parallelised codes. A performance improvement of two orders of magnitude was obtained on going from the T3D to the O2000 machines, and all the simulations described in Section 6 were performed on the latter platforms. Baseline performance for a 64^3 system running on 8 processors is 3.3 timesteps per minute for a binary oil-water system. Performance scales superlinearly out to 64 processors for 64^3 and 128^3 systems. Computational complexity increases as L^3 as one increases the linear system size L . Currently the largest attainable system size is 128^3 due to memory limitations of the O2000 machines currently available to us. However, 256^3 and 512^3 systems are attainable within the limits of the O2000 architecture. A port to the Cray T3E (MPP architecture) has also been performed, and a comparison on a processor-by-processor basis gives a performance of 30-50% of the

O2000, with linear as opposed to superlinear scalability. However, the larger number of processors available on a typical T3E system more than compensates for this relative fall off—in one case we had access to a 1200-node T3E for a period of one month. A full description of the computational aspects of this model will be provided elsewhere.

In addition to the demanding nature of the simulations themselves, visualising the results produced can be as—and in some aspects more—computationally demanding. In particular, the generation of geometrical information required to plot 3D isosurfaces of individual species concentration requires RAM resources of at least 1 Gbyte. Although visualisation is today sometimes still regarded as a subsidiary activity to numerical simulation, we have found it absolutely vital to check that the code was working, to distinguish different morphologies and to gain intuition about the very complex dynamics of these systems. Visualisation of the largest and most complex systems attainable by simulation using our hydrodynamic lattice gas demands use of the most advanced graphics engines currently available.

5 Definition of Coupling Constants

The Hamiltonian used to determine the collision outcomes has been specified in Eq. (20). We now describe the choice of the coupling constants α , μ , ϵ , ζ . In addition to the terms in Eq. (20) there is an additional kinetic energy term, so that the Hamiltonian becomes:

$$H(s') = \mathbf{J} \cdot (\alpha \mathbf{E} + \mu \mathbf{P}) + \boldsymbol{\sigma}' \cdot (\epsilon \mathbf{E} + \zeta \mathbf{P}) + \mathcal{J} : (\epsilon \mathcal{E} + \zeta \mathcal{P}) + \frac{\delta}{2} |\mathbf{v}(\mathbf{x}, t)|^2, \quad (40)$$

where \mathbf{v} is the average velocity of all particles at a site, and the mass of the particles is set to unity ($\delta = 1.0$). Our model reduces to the Rothman-Keller model for binary immiscible fluids in the limit $\alpha \rightarrow \infty$. The three remaining parameters control the surfactant interactions. These were chosen by performing an extensive parameter search using binary water-surfactant systems, and measuring the structure factor for these systems to look for signs of self-assembly. In particular, we sought strong structure-factor peaks indicative of spherical or wormlike micelles of a characteristic size were sought. These simulations were performed with a surfactant:water ratio of 1:2, well above the critical concentration for the formation of micelles. The physical contributions of each term in Eq. (20), and therefore the effect of varying each

parameter, is described below:

- ϵ controls the interaction of outgoing dipoles with the surrounding colour field. In ternary phases this term will send surfactant to oil-water interfaces. In binary water-surfactant phases this interaction will tend to favour flat interfaces between the phases;
- μ controls the interaction of outgoing coloured particles with the surrounding dipolar field. This term will favour the bending of dipoles around a central colour charge, and will be important in creating micellar phases;
- ζ controls the surfactant-surfactant interaction. For positive ζ this produces an attractive, ferromagnetic interaction between the dipoles. This term is of limited importance in the formation of self-assembled phases, and was set to 0.5 for the simulations described below.

The key to locating the micellar phases is to find the correct balance between ϵ and μ . Strongly peaked structure functions were obtained for the following values of ϵ and μ :

$$0.75 < \mu < 2.0$$

$$0.25 < \epsilon < 2.0$$

In order to maximise the desired behaviour of sending surfactant to oil-water interfaces while retaining the necessary micellar binary phases we chose a canonical set of coupling constants which are kept constant throughout all the following simulations, except in the short vesicle study described in Section 6.5. The values of these constants are:

$$\alpha = 1.0, \epsilon = 2.0, \mu = 0.75, \zeta = 0.5$$

The temperature-like parameter, β , was held constant at 1.0 for all of the ensuing simulations.

6 Simulations

The equilibrium properties and phase diagrams of a wide variety of real amphiphilic fluids are well known [14]. These phase diagrams have many features unique to three dimensional systems. To establish the general

validity of our model it is essential that we can reproduce the complex phase behaviour observed in real amphiphiles. In this section we describe some of this phenomenology, and present results of the simulations designed to reproduce it.

6.1 Oil-Water System

The spinodal decomposition of immiscible fluids has been extensively studied in two dimensions, and rather less in three [3, 15]. After a quench into the two phase region an initially homogeneous mixture separates into relatively pure single-phase domains.

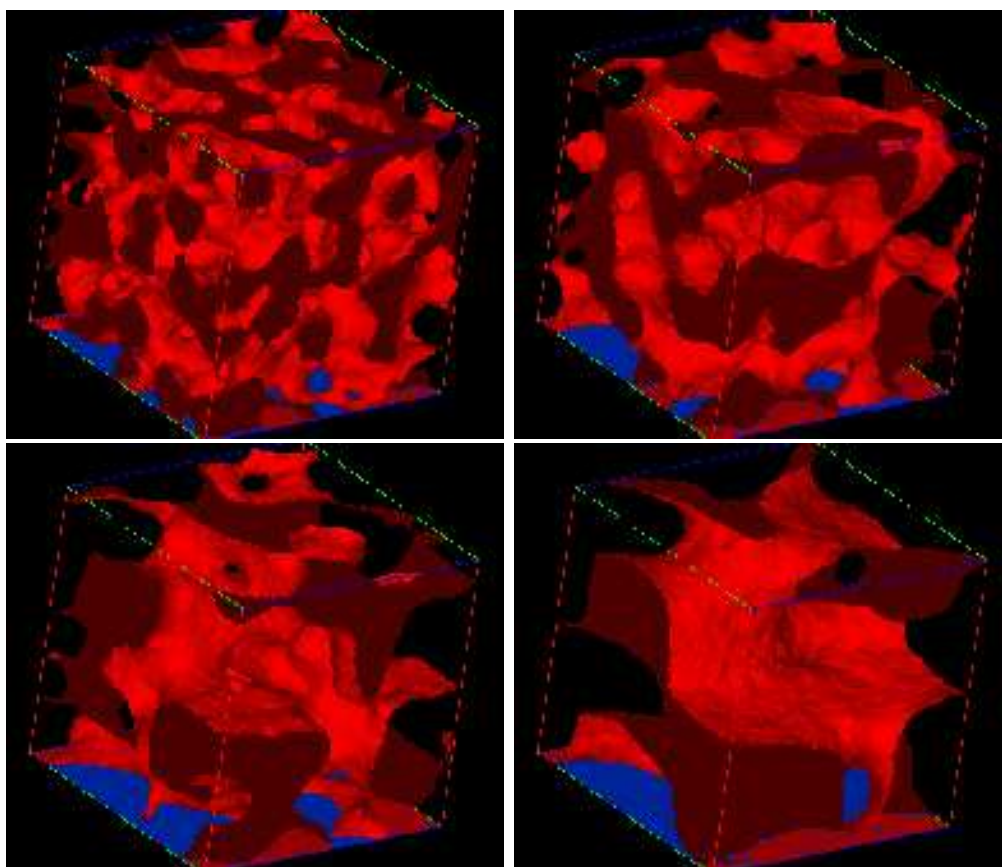


Figure 1: Binary phase separation in an oil-water system. Timesteps (clockwise from top left) 200, 400, 600, 1000. Red isosurface shows interface between oil and water phases. System size is 64^3 .

With no surfactant particles present in the system, the only term in the local site Hamiltonian, Eq. (20), that contributes numerically to the collision process is $\alpha\Delta H_{cc}$. With parameters $\alpha = 1.0$, $\beta = 1.0$ we

performed simulations starting from an initial configuration in which the lattice vectors at each site are populated randomly with oil or water particles with equal probability (a so-called critical quench). This initial condition corresponds to a homogenised 1:1 oil water mixture. The reduced density (i.e. the proportion of lattice vectors at each site that contain a particle) is 0.5. In this parameter regime, the model exhibits phase separation with positive surface tension, as is evident from Fig. 1, which illustrates the nonequilibrium behaviour of the immiscible lattice gas. If left to run for a large enough time the system would eventually reach the completely separated state of two distinct layers of fluid. To make a detailed comparison between the immiscible oil-water fluid behaviour shown here and later simulations in which we introduce surfactant to the system, we make use of *spherically averaged structure functions*. We first calculate the three-dimensional structure factor of the colour charge, $s(\mathbf{k}, t)$,

$$s(\mathbf{k}, t) = \left\langle \frac{1}{N} \left| \sum_{\mathbf{x}} (q(\mathbf{x}) - q^{av}) e^{i\mathbf{k}\cdot\mathbf{x}} \right|^2 \right\rangle,$$

where $\mathbf{k} = (2\pi/L)(p\mathbf{i} + q\mathbf{j} + r\mathbf{k})$, $p, q, r = 1, 2, \dots, L$, $q(\mathbf{x})$ is the total colour charge at a site, q^{av} is the average value of the colour charge, L is the length of the system and $N = L^3$ is the number of lattice sites in the simulation box.

We actually compute the spherically averaged structure factor, given by

$$S(k, t) = \frac{\sum_{\hat{k}} s(\mathbf{k}, t)}{\sum_{\hat{k}} 1}, \quad (41)$$

where $k = 2\pi n/L$, $n = 0, 1, 2, \dots, L$, and the sum $\sum_{\hat{k}}$ is over a spherical shell defined by $(n - \frac{1}{2}) \leq \frac{|\mathbf{k}|L}{2\pi} < (n + \frac{1}{2})$. The resolution of $S(k, t)$ depends on k_c , the Nyquist cutoff frequency associated with the lattice (for a real-space sampling interval of Δ the cut-off frequency is $1/(2\Delta)$); above this value of the frequency there is only spurious information due to aliasing. In our case, $k_c = (2\pi/L)n_c$, where we have chosen n_c to be the maximum possible value, which is half the lattice size. Fig. 2 shows the temporal evolution of $S(k, t)$ for the case of two immiscible fluids. As time increases, the peak of $S(k, t)$ shifts to progressively smaller wave numbers and its peak height increases. This behaviour is characteristic of domain coarsening and serves as a useful comparison for the surfactant-containing systems described below.

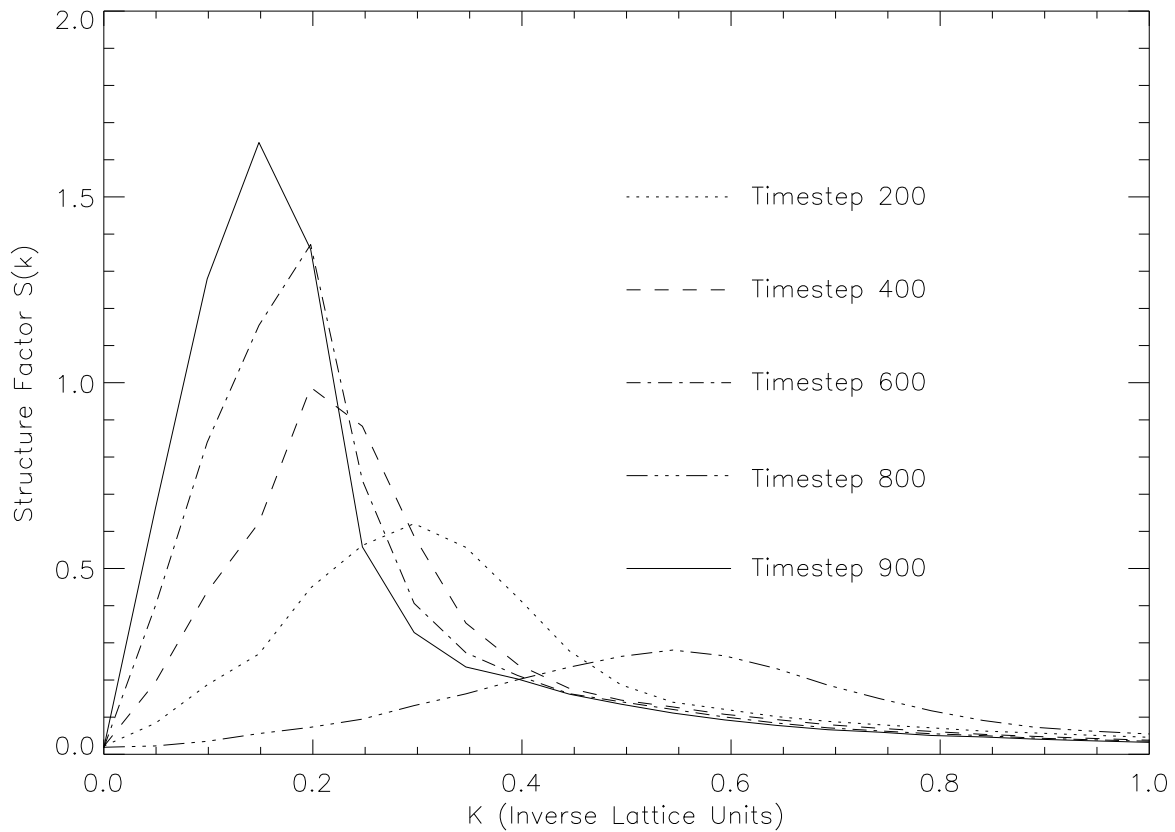


Figure 2: Structure factor for timesteps 200, 400, 600, 800, 1000 in a binary phase-separating system . System size is 128^3 . The structure factor measurements are averaged over ten independent simulations.

6.2 Binary amphiphilic fluid phases: from monomers to sponges.

In two dimensions the behaviour of the binary water-amphiphile lattice gas fluid is characterised by a *critical micelle concentration* (CMC) below which the fluid is a solution of monomeric amphiphiles, and above which the monomers form circular micelles. Further increase in amphiphile concentration in 2D simply results in more micelles, the micelles retaining their characteristic size. The situation in three dimensions is more complex. A CMC is still present for the formation of spherical micelles, but at higher concentrations new structures appear. As the concentration of surfactant increases the number of spherical micelles increases, until a second critical concentration is reached, beyond which wormlike micelles are the preferred structure. When the concentration of surfactant is high enough that both surfactant and water phases percolate throughout the system a sponge phase results. We identify this sponge phase with the L_3 phase described by Gompper and Schick [14]. These concentrations have been determined in our model for $\beta = 1$ as:

$$0.006 \leq \rho_{spherical} \leq 0.012$$

$$0.08 \leq \rho_{wormlike} \leq 0.25$$

$$0.25 \leq \rho_{L_3}$$

where ρ is the reduced density; that is, the fraction of lattice sites occupied by surfactant particles. The description of these different regimes as distinct phases, with ‘critical’ concentrations separating them, may be somewhat misleading. There is a large degree of phase coexistence. Individual monomers may join or leave a micelle in the spherical micelle regime, and the kinetics of simple micelle formation can be modelled theoretically on the basis of a Becker-Döring theory [8, 18]. The critical concentration for the formation of spherical micelles is well defined in our model, with no micelles seen below this concentration. The formation of more complex structures, however, appears to take place by more general (Smoluchowski-type) aggregation processes; wormlike micelles are formed from the coalescence of spherical micelles. Such behaviour reflects the highly dynamic nature of our model.

We performed simulations designed to access the monomeric, spherical micelle, wormlike micelle and sponge phases. All started with random initial conditions and the coupling constants defined in Section 5. To determine the stability of these structures, we calculated spherically-averaged structure functions of the

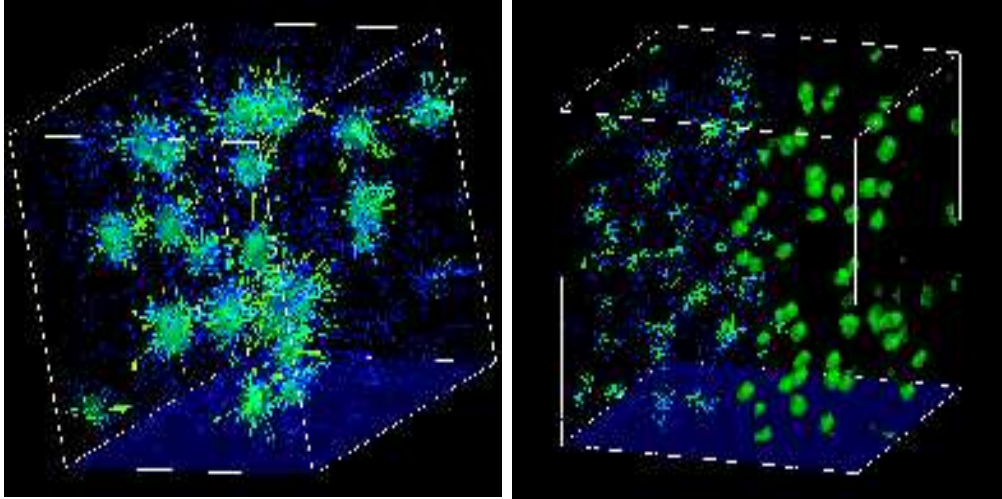


Figure 3: Spherical micelles in water at surfactant concentration 0.008, timestep 1000. Left figure shows a 32^3 system. Arrows represent the average surfactant direction per site, overlaid on an isosurface of surfactant concentration. Right figure shows a 64^3 system. The left half of this figure displays arrows of the average surfactant direction at a site, while the right half shows an isosurface of surfactant concentration.

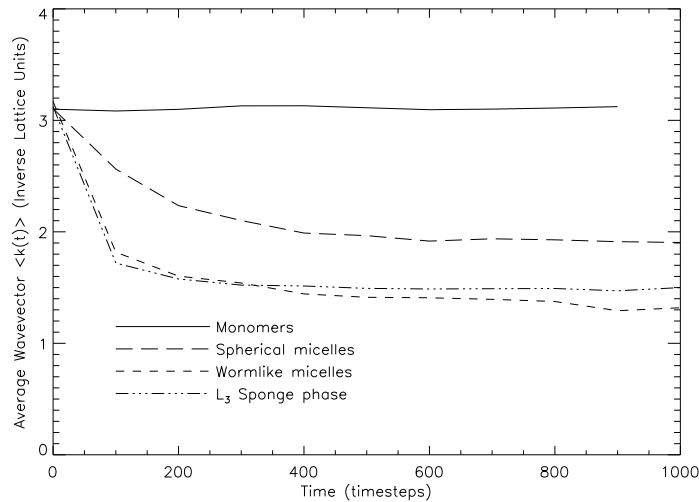


Figure 4: Average value of the magnitude of the wavevector k as a function of time for varying surfactant concentrations on a 64^3 lattice. The monomeric surfactant solution (solid line) is at reduced surfactant concentration of 0.001; spherical micelles at reduced surfactant concentration of 0.01; wormlike micelles at reduced surfactant concentration of 0.1; and the L_3 sponge phase at reduced surfactant concentration of 0.3

surfactant density. In Fig. 4, we plot the temporal evolution of the characteristic wave number,

$$\langle k(t) \rangle = \frac{\sum_{k=0}^{k_c} k S(k, t)}{\sum_{k=0}^{k_c} S(k, t)},$$

the inverse of which is a measure of the average domain size. We see that in the low amphiphile concentration case the characteristic size remains consistent with a random configuration of solubilised monomers. For the cases where visualisation establishes the presence of more complex structures there is fast initial growth of the surfactant domains which soon levels off to some constant size; see Figs 5 and 6.

6.3 Ternary phases: lamellae

We first investigate the stability of a lamellar structure, which is composed of alternating layers of oil-rich and water-rich phases separated by a monolayer of surfactant molecules. We look at the system with and without surfactant present in order for a comparison to be made. It is not clear what influence surfactant will have on such a lamellar structure in three dimensions. We are interested in the ability of surfactant to stabilise large areas of interface by lowering the interfacial tension. We set up the initial configuration of the system, with layers of oil and water four sites wide, all sites having a reduced density of 0.5. It is clear that if our model is exhibiting the correct behaviour, then we would expect there to be a critical density of surfactant required at the oil-water interfaces in order for the layered structure to be stable. Consequently, we set up a simulation with a single site wide layer of surfactant at each of the oil-water interfaces. Snapshots from these simulations are shown in Figs. 7 and Fig. 8; the former is the pure oil-water case with coupling coefficient $\alpha = 1.0$ and inverse temperature $\beta = 1.0$, while the latter has surfactant monolayers present.

The fluctuations present in the model enable oil and water particles from the initially separated layers to move; they thus come under the influence of the colour field gradients produced by other layers of the same fluid type. For these parameter choices there is an inherent tendency for the oil and water to act as immiscible fluids and phase separate (*cf.*, Fig. 1), precisely as is shown in Fig. 7. Fig. 8 shows the case where surfactant monolayers coat the oil-water interfaces. Here we see that the initial periodic structure is stabilised despite the presence of large amounts of oil-water interface.

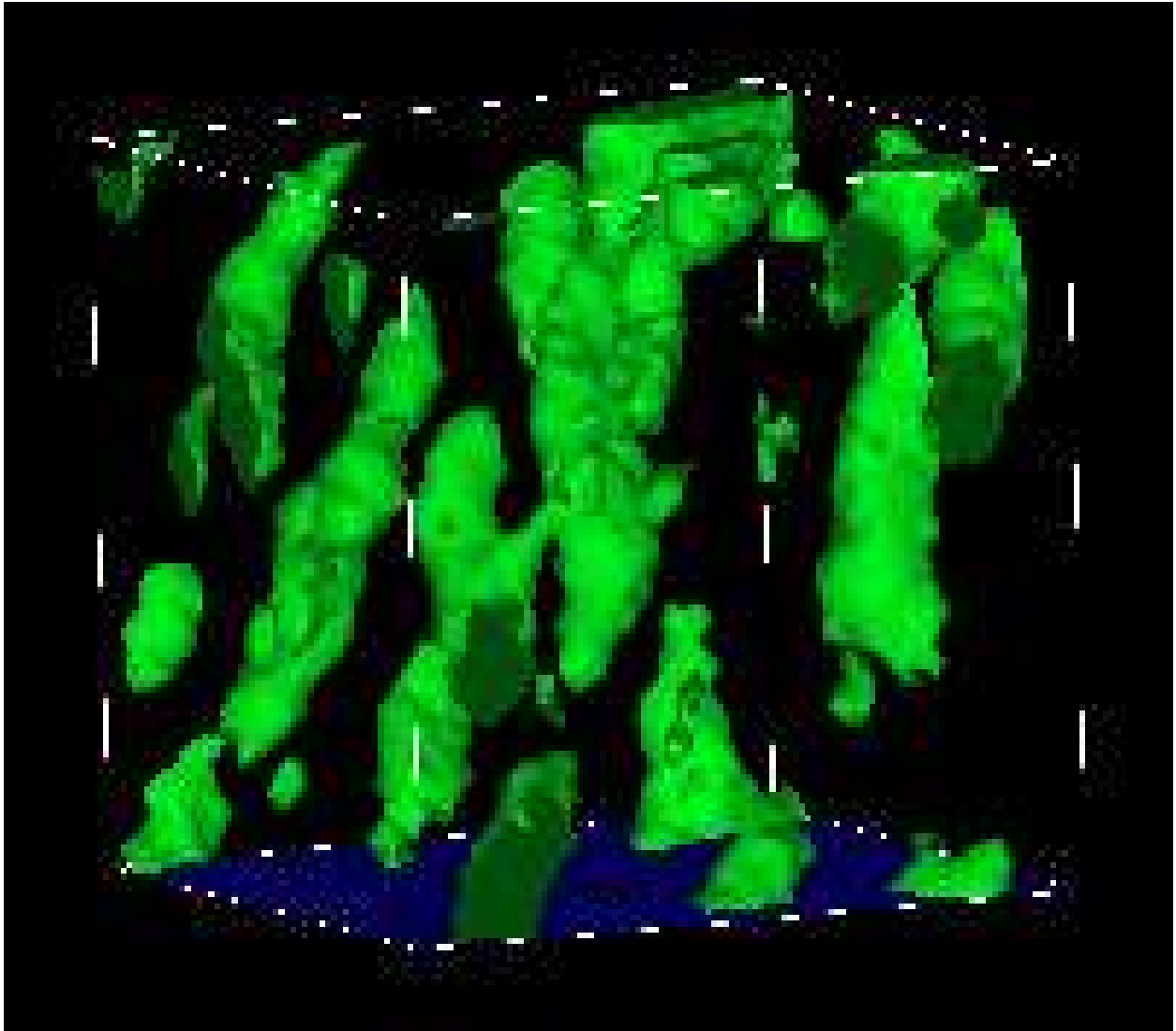


Figure 5: Wormlike micelles in water at a reduced surfactant concentration of 0.1 for a 32^3 system. The same structures are present in larger systems, but we display this snapshot for clarity. The green isosurface shows the surfactant concentration at a level of 5 particles per lattice site.

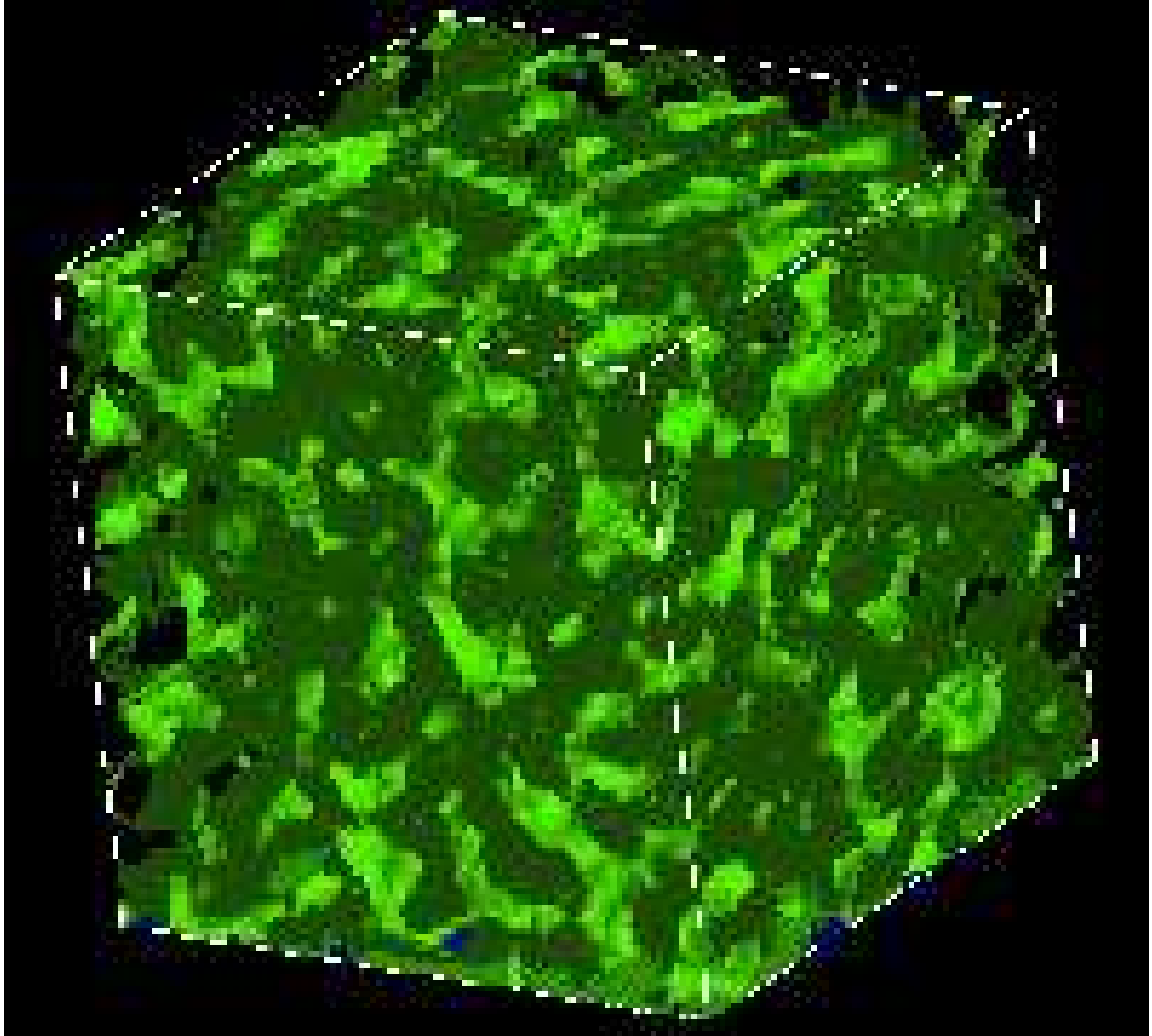


Figure 6: L_3 sponge phase at a reduced surfactant concentration of 0.3. The green isosurface shows the surfactant concentration at a level of 5 particles per site. The system size is 64^3 .

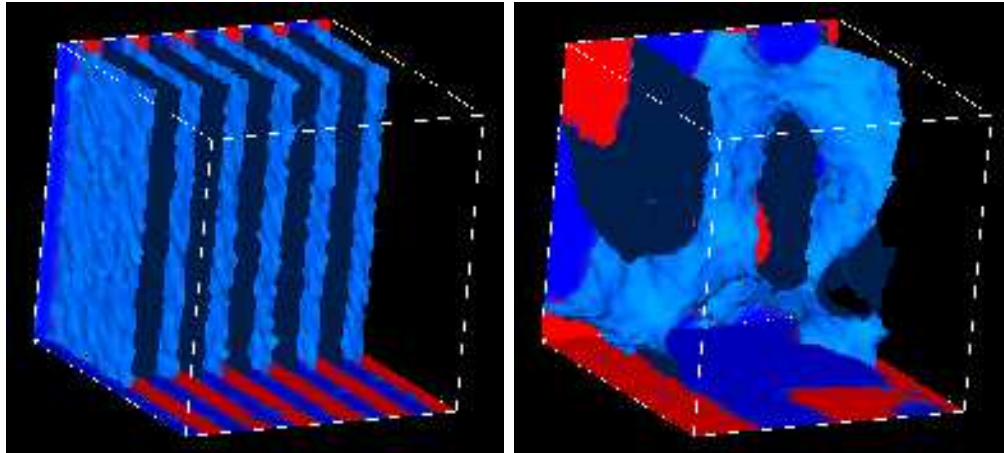


Figure 7: Binary oil-water lamellae at timesteps $t = 0$ (left) and $t = 500$ (right) for a 48^3 system. The red and blue colourings on the slice planes indicate oil and water respectively, while the blue isosurface shows the interface between oil and water. For clarity the isosurface is shown for only half of the system. The system size is 48^3

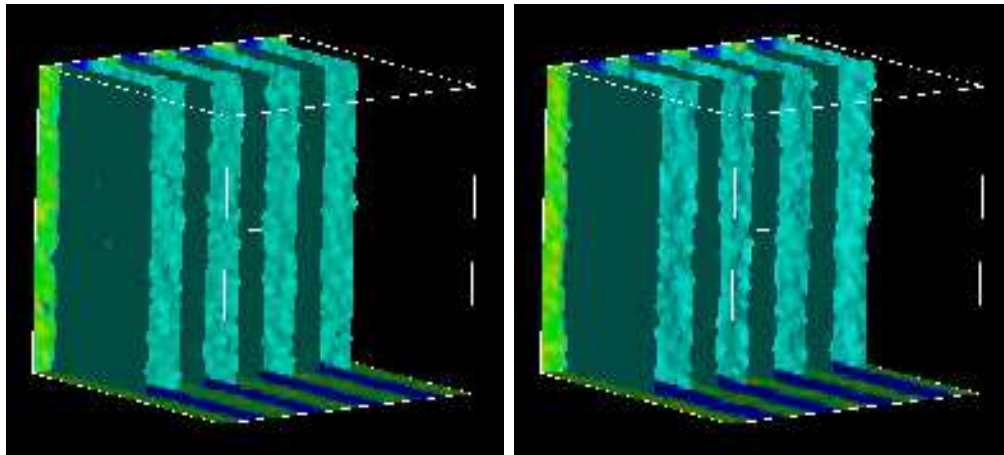


Figure 8: Ternary lamellae at $t = 0$ (left), and $t = 1000$ (right). The isosurface shows the oil-water interface. System size is 40^3 .

6.4 Ternary phases: oil-in-water (water-in-oil) and bicontinuous microemulsions.

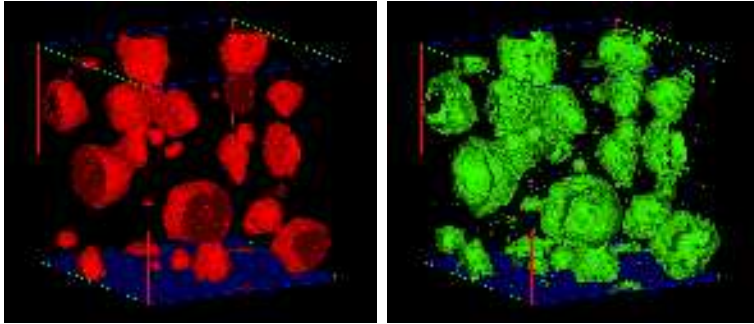


Figure 9: Oil-in-water droplet phase arising from a random initial condition. Oil (red, left) and surfactant (green, right) isosurfaces.

The ternary behaviour of amphiphilic systems shows the same increase in complexity between two and three dimensions that we have seen in the binary water-surfactant systems. One simplifying feature of our model is the symmetry between oil and water in the interactions producing the phase behaviour. We discuss here the two most basic of the many ternary phases, the oil-in-water droplet and the bicontinuous *microemulsion* phases.

In the oil-in-water droplet phase, oil exists as the minority phase in a continuous background of water and surfactant. If sufficient surfactant is present in the system the spinodal decomposition of a quenched uniform mixture of the three components will be arrested, and the system will reach an equilibrium state consisting of droplets of oil in water with surfactant stabilising the oil-water interfaces. This phase may be regarded as a perturbation of a binary spherical micelle phase, the micelles now being swollen with oil. If one increases the oil concentration, a regime is reached where both the oil and water domains percolate throughout the system. Such a phase is the ternary extension of the L_3 sponge phase in the binary system.

In both these cases, the complete separation of the oil and water phases, which is the equilibrium state for a binary immiscible fluid, is prevented by the presence of the surfactant. In order to quantify this result, and to compare with the previous binary case, we calculate the mean k value of the spherically averaged structure factor of the colour charge, and plot the result in Fig. 10.

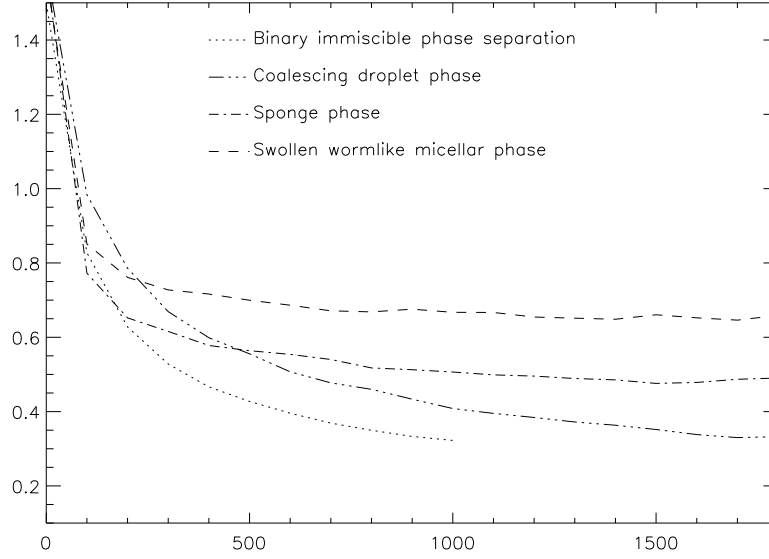


Figure 10: Structure factor mean k value for binary phase separation, ternary coalescing droplet phase, swollen wormlike micellar phase, and bicontinuous microemulsion phases.

In order to reproduce the oil-in-water droplet phase, we set up two simulations with a random initial configuration and a reduced density of oil of 0.05. The concentration of surfactant was varied between the two simulations, the reduced surfactant density being 0.01 and 0.21 respectively. The total reduced density for both simulations was 0.5; to maintain consistency between our various simulations, we continue to use the numerical values for the coupling constants defined in Section 5.

Fig. 9 displays a snapshot of the simulation with a reduced surfactant density of 0.01 at timestep 1000, displaying the oil (red) and surfactant (green) isosurfaces. It is clear that the surfactant is adsorbed at the interface. However, Fig. 10 shows the time evolution of the average k value of the spherically averaged structure factor. It is clear that although the phase separation is slowed by the presence of surfactant, the average domain size in the system is increasing with time. For the case with reduced surfactant density 0.21, one observes complete arrest of phase separation, with wormlike oil domains remaining at a constant size as shown by the dashed line in Fig. 10. We refer to this morphology as a swollen wormlike micellar phase. A snapshot of this simulation taken at timestep 4000 is shown in Fig. 11.

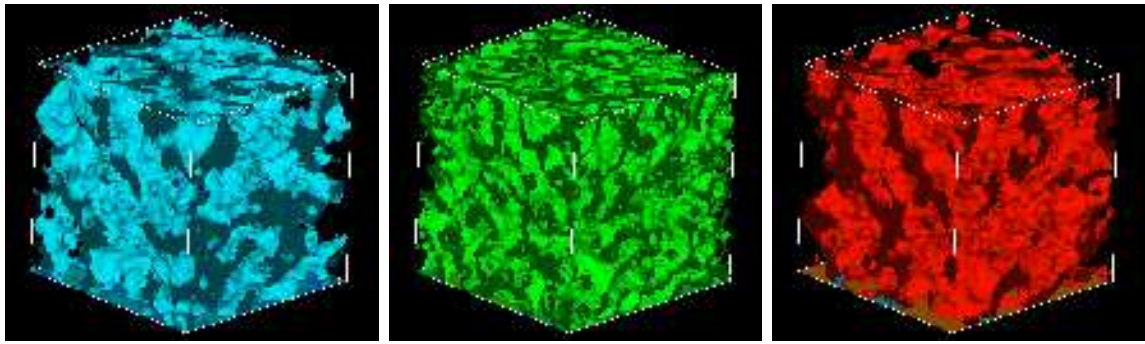


Figure 11: Bicontinuous microemulsion phase at timestep 4000. Left: water isosurface; middle: surfactant isosurface; right: Oil isosurface. The system size is 64^3 . Isosurfaces display concentrations of water, surfactant and oil, respectively, at a level of five particles per site.

To obtain the bicontinuous sponge regime within the model's phase diagram, we simply increase the relative amount of oil present in the system. Hence this simulation has a random initial mixture with a reduced density 0.5 and a 0.83 : 1.0 : 0.83 oil-to-surfactant-to-water ratio. Fig. 12 displays the results of this simulation at timestep 4000, displaying the percolating oil (red) and water (blue) isosurfaces, as well as the surfactant (green) isosurface.

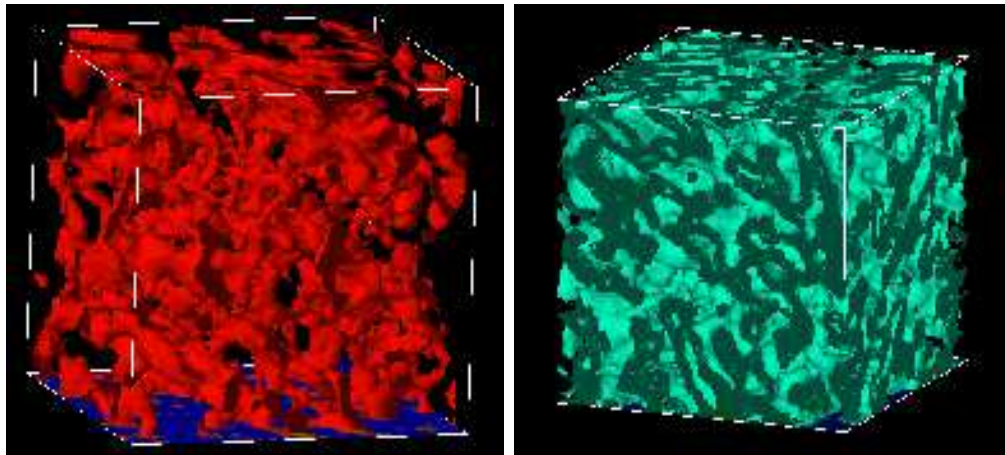


Figure 12: Stable oil-in-water droplet phase at timestep 4000. Red and green isosurfaces show oil and surfactant concentrations at a level of five particles per site. The system size is 64^3 .

These results show the ability of our model to correctly reproduce the effects of surfactant on the phase

separation dynamics of binary immiscible fluids. A quantitative study of the domain growth behaviour for both binary and ternary systems will be described in a future paper.

6.5 Vesicles

Membrane theory treatments of amphiphilic systems predict that for large binary water surfactant systems a bilayer can reduce its energy by closing its boundary, creating a large structure known as a vesicle [14]. Such structures can exist because the energy required to bend the bilayer into a sphere is less than that required to maintain the bilayer edge. We do not expect vesicles to self-assemble in our current simulations, in part because such structures are usually metastable in real life and require the input of energy, for example via shearing or sonication. We can, however, construct such a structure as an initial condition and study its stability, or lack thereof, using our model. The initial condition we have used is shown in Fig. 13. The concentration of surfactant is initially zero except within a spherical shell, 5 sites wide and 32 sites in radius, where the reduced density of surfactant is 1.0. All other sites contain water particles with a reduced density of 0.5. The total system size is 128^3 .

For the following simulations, we have not used the canonical choice of coupling constants described in Section 5. Rather, in order to study the mechanisms by which these vesicles disintegrate, we have performed three separate simulations, with the following parameter choices:

$$\alpha = 1.0, \epsilon = 0.01, \mu = 0.01, \zeta = 1.0$$

$$\alpha = 1.0, \epsilon = 0.01, \mu = 1.00, \zeta = 0.01$$

$$\alpha = 1.0, \epsilon = 1.00, \mu = 0.01, \zeta = 0.01$$

These three simulations should separate the effects of the three surfactant interactions on the vesicles. We also wish to characterise the timescale over which the vesicles are stable. In order to do this, we performed one simulation with oil particles replacing the surfactant particles in the initial condition, and with $\alpha = 0.0$. This essentially labels the particles starting in the vesicle region, and allows us to track their subsequent motion. Not surprisingly, this simulation shows that the initial vesicle configuration is destroyed in the absence of interactions in less than ten timesteps. The initial condition and state of the system at timestep

200 for the above three simulations is shown in Fig. 13. These simulations show that the mechanisms driving the breakup of the vesicles are phase separation and micellisation. The vesicles are also unstable against fluctuations in concentration which produce holes in the structure. Once a hole has been produced it is observed to grow until the vesicle is destroyed.

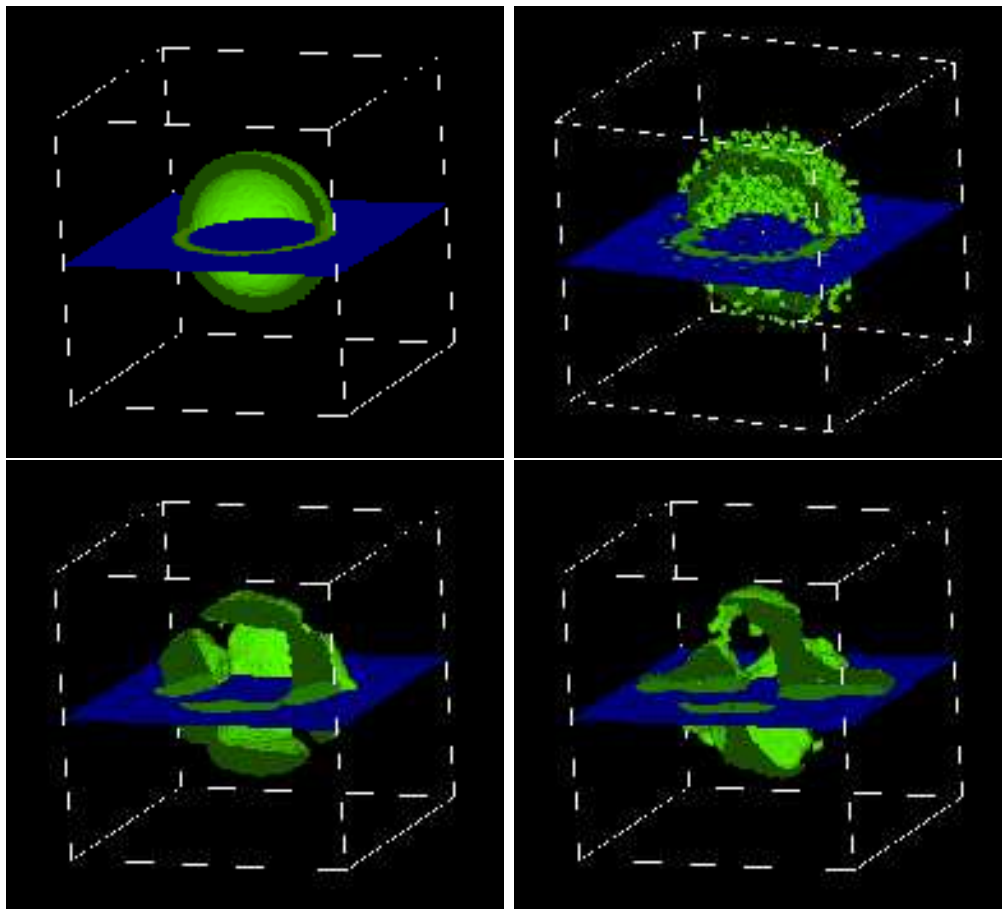


Figure 13: Vesicle disintegration. Clockwise from top left: Initial condition. Simulation with $\epsilon = 0.01$, $\mu = 1.00$, $\zeta = 0.01$ at timestep 200. Simulation with $\epsilon = 1.00$, $\mu = 0.01$, $\zeta = 0.01$ at timestep 200. Simulation with $\epsilon = 0.01$, $\mu = 0.01$, $\zeta = 1.0$ at timestep 200. All snapshots display an isosurface showing reduced surfactant density at a level of 5 particles per site for half the vesicle.

7 Conclusions

We have extended our hydrodynamic lattice-gas model for the dynamics of binary and ternary amphiphilic fluids from two to three dimensions. We have shown that our model exhibits the correct 3D phenomenology using a combination of visual and analytic techniques. Experimentally observed self-assembling structures form in our simulations in a consistent manner when the relative concentrations of the three components are varied. Binary immiscible, binary amphiphilic and ternary amphiphilic behaviour are all captured using a single set of coupling constants. We have also shown that studies of vesicle metastability are possible using this model with different choices of the coupling constants. Work is currently in progress on a wide range of amphiphilic fluid systems, including measurements of viscosity and surface tension, and the study of growth laws in amphiphilic self-assembly processes. Studies of amphiphilic fluid flow in porous media, which have previously been performed in 2D [7], are now underway using the 3D model [6]. Indeed there is a rich seam of problems related to amphiphilic fluids which may be mined using this model. Our work confirms the suitability of lattice gas automata for the modelling and simulation of such complex fluid problems in both two and three dimensions.

Acknowledgements

We are indebted to numerous people and organisations for their support of and contributions to this work. They include Jean-Bernard Maillet and David Bailey at Schlumberger Cambridge Research, Silicon Graphics Incorporated (particularly Bart van Bloemann Waanders, Daron Green and Rob Jenkins), Oxford Supercomputing Centre (particularly Jeremy Martin and Kathryn Measures), the EPSRC E7 High Performance Computing Consortium (particularly Sujata Krishna), the Edinburgh Parallel Computing Centre (particularly Mario Antonioletti), and the National Computational Science Alliance in Illinois, USA. PJJ would like to thank EPSRC and Schlumberger Cambridge Research for funding his CASE studentship award. The collaboration between PVC and BMB was supported by NATO grant number CRG950356. BMB was supported in part by the United States Air Force Office of Scientific Research under grant number F49620-95-1-0285.

References

- [1] Adler, C., Boghosian, B.M., Flekkøy, E.G., Margolus, N., Rothman, D.H. 1995 *J. Stat. Phys.* **81**, 105-128.
- [2] Boghosian, B.M., Coveney, P.V. and Emerton, A.N. 1996 *Proc. Roy. Soc. A* **452**, 1221-1250.
- [3] Bray, A.J. *Adv. in Physics* 1994, **43**, 357-459
- [4] Cazabat, A.M., Langevin, D. Meunier, J. & Pouchelon, A. 1982 *Adv. Colloid Interface Sci.* **16**, 175-199.
- [5] Chan, C.K. & Liang, N.Y. 1990 *Europhys. Lett.* **13**, 495-500.
- [6] Coveney, P.V., “Lattice gas simulation of enhanced oil recovery using high performance computing” 1999 SGI High Performance Visualisation and Computing Summit, Galveston, Texas, USA, 18-20 January
- [7] Coveney, P.V., Maillet, J.-B., Wilson, J., Fowler, P.W., Al-Mushadani, O., & Boghosian, B.M. 1998 *Int. J. Mod. Phys.* **9**, 1479-1490.
- [8] Coveney, P.V. & Wattis, J.D. 1996 *Proc. Roy. Soc. A* **452** 2079.
- [9] A.N. Emerton, P.V. Coveney, & B.M. Boghosian 1996 *J. Amer. Chem. Soc.* **118** , 10719-10724
- [10] A.N. Emerton, P.V. Coveney & B.M. Boghosian 1997 *Phys. Rev. E* **55**, 708.
- [11] A.N. Emerton, P.V. Coveney & B.M. Boghosian 1997 *Physica A.* **239** , 373.
- [12] A.N. Emerton, F.J. Weig, P.V. Coveney & B.M. Boghosian, 1997 *J. Phys. Cond. Mat.* **42** , 8893-8905.
- [13] Frisch, U., d’Humières, D., Hasslacher, B., H. Lallemand, P., Pomeau, Y. & J-P. Rivet 1987 *Complex Systems.* **1**, 1-31.
- [14] Gompper, G. & Schick, M. 1994 *Phase Transitions and Critical Phenomena* **16** 1-181
- [15] Jury, S.I., Bladon, P., Krishna, S. & Cates, M.E. 1999 *Phys. Rev. E* **59** R2535-R2538.
- [16] Kahlweit, M. Strey, R. Haase, D. Kuneida, H. & Schmeling, T. 1987 *J. Colloid Interface Sci.* **118**, 436.

- [17] Kawakatsu, T., Kawasaki, K., Furusaka, M., Okabayashi, H. & Kanaya, T. 1993 *J. Chem. Phys.* **99**, 8200-8217.
- [18] J-B Maillet, V. Lachet, P.V. Coveney, 1999 “Large scale molecular dynamics simulations of self-assembly processes in short and long chained surfactant systems”, preprint.
- [19] Palmer, B.J. & Lin, J. 1996 *Langmuir* **12**, 746-753.
- [20] Rothman, D.H. & Keller, J.M. 1988 *J. Stat. Phys.* **52**, 1119-1127.
- [21] Wolfram, S. 1986 *J. Stat. Phys.* **45**, 471-526.
- [22] Smit, B. Hilbers, P.A.J. Esselink, K. Rupert, L.A.M. van Os, N.M. Schlijper, A.G. 1991 *J. Phys. Chem.* **95**, 6361-6368.